RSC Advances

PAPER

View Article Online
View Journal | View Issue

Cite this: *RSC Adv.*, 2025, **15**, 50470

Simultaneous electrochemical detection of Cu, Cd and Mn by nickel ferrite–cobalt ferrite bimetallic nanocomposite

Zahid Ali,[a] Jameel Ahmed Baig,[b] Hassan Imran Afridi,[a] Khalil Akhtar,*[a] Saima Perveen[a] and Nadeem Raza[b]

Received 25th October 2025
Accepted 2nd December 2025

DOI: 10.1039/d5ra08189k

rsc.li/rsc-advances

The current study focuses on the synthesis of nanomaterials for fabrication of electrochemical sensors for the simultaneous detection of toxic metals, such as Cd, Cu, and Mn. Nickel and cobalt ferrite nanoparticles were synthesized by the sol–gel method and then combined by the green method to obtain a nickel ferrite–cobalt ferrite nanocomposite ($NiFe_2O_4$·$CoFe_2O_4$-NC) for electrochemical sensing of Cd, Cu and Mn. The characterization of the synthesized $NiFe_2O_4$·$CoFe_2O_4$-NC confirmed its coral-like shape with a highly rough and porous structure, cubic-spinel phase, crystalline size (<23.1 nm), good stability and electronic properties. $NiFe_2O_4$.$CoFe_2O_4$-NC/GCE was fabricated and showed good sensitivity due to its large electroactive surface area, fast electron transfer rate, and powerful electrocatalytic activity, which were beneficial for the quantitative determination of Cd, Cu and Mn. The $NiFe_2O_4$·$CoFe_2O_4$-NC/GCE showed the limit of detection of 0.083, 0.188 and 0.026 μg L^{-1} for Cd, Cu and Mn, respectively. The proposed sensor was successfully applied for the analysis of Cd, Cu and Mn in tap water, mango juice, and milk samples, which confirmed its excellent efficiency with RSD < 4.0%.

1 Introduction

Environmental pollution is increasing every day due to the release of several substances, including toxic metals (TMs), dyes, pesticides, pharmaceuticals, and other chemical residues that contaminate the environment.[1,2] Among them, the study of TMs is quite important for food safety, environmental protection, and human health. The study of TM pollution also holds importance in the field of agriculture and industries for controlling environmental pollution.[3] Many TMs, such as cadmium (Cd), copper (Cu), and manganese (Mn), have a specific role in many aspects of the environment and life. However, their excess levels can harm human health and the environment. For example, Cd has several industrial applications, notably in batteries, pigments, and as a coating, but its improper disposal in the environment can damage the lungs, liver, induce osteotoxicity and nephrotoxicity, pulmonary adenocarcinomas, prostatic proliferative lesions, pulmonary adenocarcinomas and disturb the immune system of the body.[4–6] Furthermore, trace levels of Cu play a significant role in the physiological function of the human body. Still, little excess intake of Cu can have unfavorable effects on humans, such as disrupting the intestine, liver and stomach,[7,8] and if swallowed in higher concentrations, can lead to skin cancer, dermal lesions, angiosarcoma, peripheral neuropathy, and vascular disease.[9] Moreover, Mn plays an important role in the metabolism of carbohydrates, cholesterol, and amino acids, and higher concentrations can cause numerous diseases such as male infertility, neurological disorders, birth disability, and bone defects.[10]

Several methods have been reported up to now for detecting these TMs, including complexometric titration,[11] chromatography,[12] chemiluminescence,[13] and spectrophotometry.[14] But the sophisticated procedures, time-intensive nature, and expense of these methods limit their suitability for routine analysis. Fortunately, voltammetry is a simple, fast, and low-cost alternative to other reported methods.[15–17] It stands out due to its ultra-high sensitivity, simultaneous detection of multiple metals, preconcentration capability, and improved selectivity for analysis of TMs. The stripping mode of voltammetry is mainly beneficial for analyzing trace and ultra-trace metals. Despite these benefits, the voltammetric techniques may have limitations such as unstable response in complex matrices, no response for electrochemically inactive species, or thermodynamically predicted to undergo heterogeneous redox. These limitations are subject to the analysis of electrolytes that may be restricted to the aqueous medium and inappropriate potential ranges for targeted analytes.[18] The selection of Cd, Cu, and Mn in the present work is not only due to their environmental and health relevance but also because these metals exhibit sufficiently distinct redox potentials, allowing clear and

[a]*Centre of Excellence in Analytical Chemistry, University of Sindh, Jamshoro 76080, Pakistan. E-mail: khalil.akhtar@scholars.usindh.edu.pk*

[b]*Department of Chemistry, College of Science, Imam Mohammad Ibn Saud Islamic University (IMSIU), Riyadh, Saudi Arabia*

non-overlapping voltammetric peaks. This inherent electrochemical separation makes them particularly suitable for simultaneous detection using modified electrodes. However, despite its advantages, voltammetric analysis can encounter challenges, such as unstable responses in complex matrices, limited applicability for electrochemically inactive species, and constraints arising from electrolyte composition or limited potential windows.[18]

Further, the chemical modification of these electrodes has been demonstrated to be the most effective for trace-level metal measurement due to their sensitivity, selectivity, stability, and versatility. The chemically modified electrodes (CMEs) offer lower detection limits, extended operational lifespans and greater complexity handling. These advantages make CMEs valuable for environmental monitoring, pharmaceutical testing, and industrial quality control applications. For the development of CME, a thin film of desired chemicals is coated onto the electrode surface to provide the required film properties. Various materials are employed as chemical modifiers to enhance the sensitivity of electrodes, such as gold nanoparticles (Au-NPs),[19] sodium ferrite nanoparticles ($Na_2Fe_4O_7$-NPs),[20] magnesium nanoferrites ($MgFe_4O_7$-NPs),[21] and copper oxide/tin oxide nanoparticles (CuO/SnO_2-NPs).[22] Although several materials such as graphene, carbon nanomaterials, and biopolymers (*e.g.*, chitosan) are commonly used to enhance charge-transfer properties of sensor surfaces, ferrite-based nanocomposites offer additional benefits that justify their use in this work. Ferrite nanoparticles possess tunable structure, high porosity, large surface area, chemical stability, and strong electrocatalytic activity. When combined to form ferrite nanocomposites (FNCs), the synergistic interaction between multiple ferrite phases further enhances electron-transfer kinetics, increases the density of active sites, and improves selective binding toward metal ions. These combined features provide higher sensitivity, better peak resolution, and improved operational stability compared to many single-component modifiers. Therefore, using $NiFe_2O_4 \cdot CoFe_2O_4$ nanocomposite enables superior electrochemical performance for simultaneous detection of Cu, Cd, and Mn at trace levels.[20–22]

Ferrite based nanoparticles (FNPs) are ideal and superior for a wide range of applications due to their cost-effectiveness, easy synthesis, high sensitivity, and selectivity. FNPs are emerging nanomaterials that have been broadly employed due to their easy modification, tunable structure, high porosity, and large surface area.[21] To further enhance the electrochemical performance, these FNPs are combined with various materials to synthesize their composites. The outstanding electrocatalytic performance and high specific surface area of FNCs make them desirable for applications in absorbents, biomedicine, electronic devices, and sensors.[21] As, $ZnFe_2O_4$/SPE sensor have applied for excellent electrochemical sensing of paracetamol.[23] Different transition FNPs (MFe_2O_4, M = Cu, Co, Ni, Zn) integrated into a polyaniline/Nafion polymer matrix with immobilized enzyme demonstrated significantly enhance biosensor response compared to bare polymer systems indicating enhanced electron transfer and favorable surface interactions provided by ferrite FNPs.[24] The FNPs are attractive for electrochemical sensors and biosensors because of their high surface to volume ratio, chemical stability, tunable surface chemistry, and ability to facilitate adsorption and enrichment of analytes at the electrode interface.[25,26]

Thus, the current study was considered to synthesize a nickel–cobalt ferrite nanocomposite ($NiFe_2O_4 \cdot CoFe_2O_4$-NC). The $NiFe_2O_4 \cdot CoFe_2O_4$-NC was thoroughly characterized by advanced analytical techniques to which confirm coral-like shape with a highly rough and porous structure, cubic crystalline structure with particle size of 53.7 nm. The synthesized $NiFe_2O_4 \cdot CoFe_2O_4$-NC was coated on the surface of GCE to fabricate electrochemical sensor ($NiFe_2O_4 \cdot CoFe_2O_4$-NC/GCE) for simultaneous detection of TMs, including Cu, Cd, and Mn in tap water and milk samples. The method showed acceptable performance with excellent stability and reproducibility. In this study, the target analytes were Cu, Cd, and Mn ions, which represent the most stable and soluble oxidation states of copper, cadmium, and manganese in aqueous media under the experimental conditions used.

2 Experimental work

2.1 Chemicals

The analytical grade chemicals were accessed from Fluka (Bush, Switzerland), including the iron nitrate $Fe(NO_3)_3 \cdot 9H_2O$, nickel nitrate $Ni(NO_3)_2$, ethanol (C_2H_5OH), potassium chloride (KCl) and Nafion for experimental work. Phosphoric acid (H_3PO_4), sodium hydroxide (NaOH), boric acid (H_3BO_3), di-sodium hydrogen phosphate (Na_2HPO_4), sodium phosphate monobasic dehydrate ($NaH_2PO_4 \cdot 2H_2O$), sodium acetate (CH_3-CHOONa), copper chloride ($CuCl_2$), cadmium chloride ($CdCl_2$), manganese chloride ($MnCl_2$), potassium ferricyanide; $K_3[Fe(CN)_6]$, acetic acid(CH_3COOH), hydrochloric acid (HCl) were obtained from Sigma-Aldrich, USA. Deionized (DI) water was obtained from the plant of the Centre of Excellence in Analytical Chemistry, Jamshoro, Pakistan.

2.2 Synthesis of ferrite ($NiFe_2O_4$ and $CoFe_2O_4$) nanoparticles

Ferrite nanoparticles ($NiFe_2O_4$ and $CoFe_2O_4$) were synthesized with slight modification using sol–gel auto-combustion technique.[27] For the preparation of $NiFe_2O_4$ nanoparticles, appropriate amount of $Fe(NO_3)_3 \cdot 9H_2O$ and $Ni(NO_3)_2$ were taken in 500 mL water and ascorbic acid is added as a fuel agent. The pH of the mixture was adjusted between 8 and 11 using ammonium hydroxide. The resulted mixture was heated on an electric hotplate at 250 °C until water is evaporated and fine powder of $NiFe_2O_4$ is obtained. The obtained product was finely ground and calcined at 900 °C for 5 hours to achieve a well crystallized $NiFe_2O_4$ phase. The yield of $NiFe_2O_4$ is obtained 81.64%.

Similarly, $CoFe_2O_4$ nanoparticles were synthesized using the stoichiometric ratio of $Fe(NO_3)_3 \cdot 9H_2O$ and $Co(NO_3)_2$ in a 500 mL beaker. The solution was heated at 250 °C on an electric hotplate to yield a brownish powder, which was then calcined at 800 °C for 5 hours to obtain phase $CoFe_2O_4$ and the yield of $CoFe_2O_4$ is obtained 83.19%. The synthesized $NiFe_2O_4$

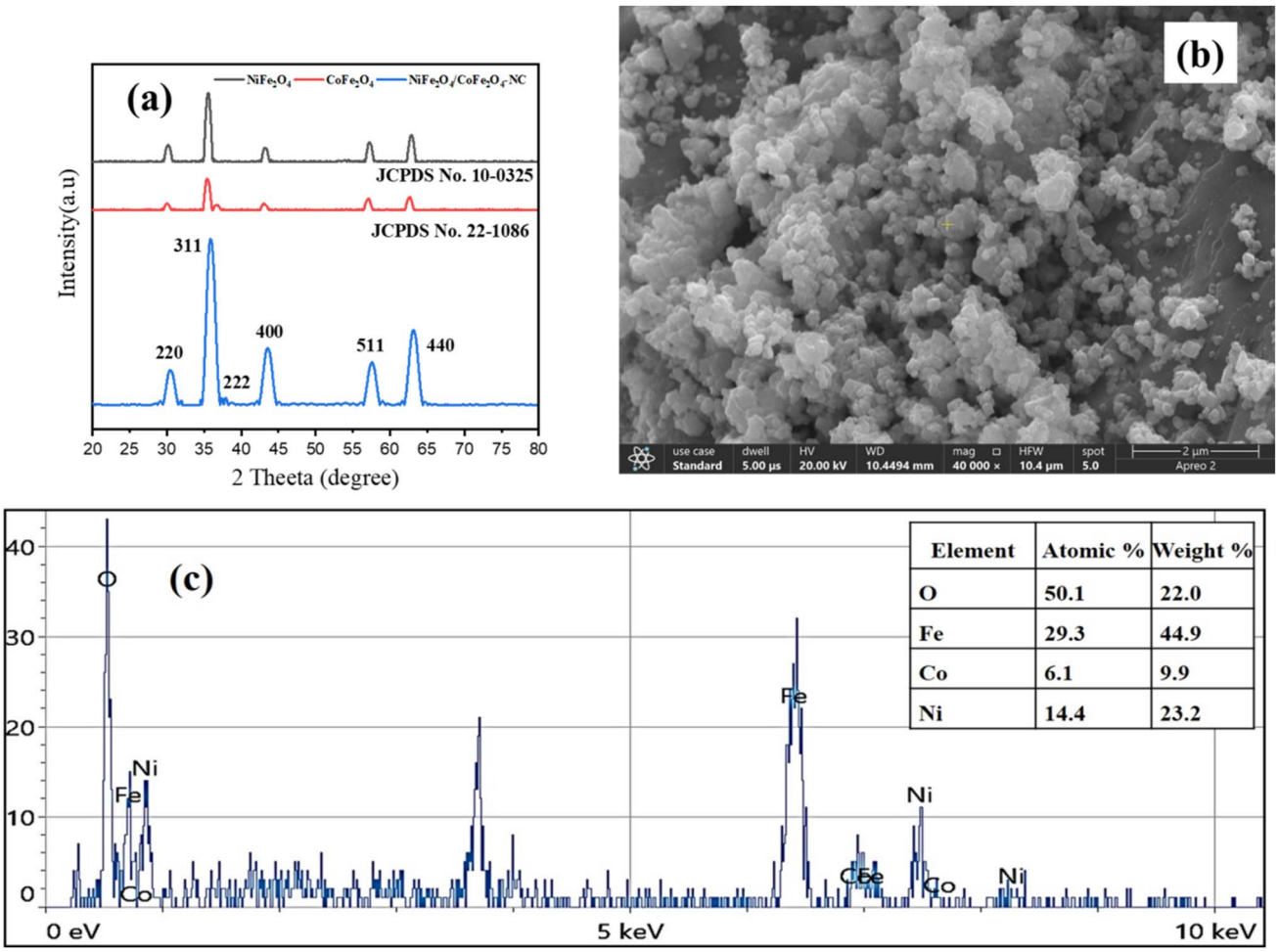

Fig. 1 (a) XRD, (b) SEM, and (c) EDX analysis of synthesized $NiFe_2O_4 \cdot CoFe_2O_4$-NC.

and $CoFe_2O_4$ nanoparticles were used to synthesize $NiFe_2O_4 \cdot CoFe_2O_4$-NC.

2.3 Synthesis of $NiFe_2O_4 \cdot CoFe_2O_4$-NC

The $NiFe_2O_4 \cdot CoFe_2O_4$-NC was synthesized by mixing of $NiFe_2O_4$ and $CoFe_2O_4$ in a 2 : 1 ratio respectively. The obtained mixture was thoroughly ground using a mortar and pestle for 15 hours, followed by calcination in a muffle furnace at 900 °C for 5 hours.[27,28] The prepared $NiFe_2O_4 \cdot CoFe_2O_4$-NC was then characterized using advanced spectroscopic techniques and utilized for the fabrication of an electrochemical sensor.

2.4 Modification of $NiFe_2O_4 \cdot CoFe_2O_4$-NC based glassy carbon electrode ($NiFe_2O_4 \cdot CoFe_2O_4$-NC/GCE)

The GCE is polished with 0.05 µm alumina slurry, sonicated in DI water for 10 minutes, then rinsed with ethanol.[29] For the fabrication of $NiFe_2O_4 \cdot CoFe_2O_4$-NC/GCE, a suspension was prepared by dispersing 2 mg of $NiFe_2O_4 \cdot CoFe_2O_4$-NC in 2 mL of DI water containing 50 µL of Nafion, and sonicated for 15 min. Subsequently, 10 µL of the prepared suspension was drop cast onto the surface of the GCE and dried overnight at room temperature. This process resulted in the formation of a stable, uniformly immobilized layer of $NiFe_2O_4 \cdot CoFe_2O_4$-NC on the surface of GCE.[30]

2.5 Electrochemical measurements

$NiFe_2O_4 \cdot CoFe_2O_4$-NC/GCE is employed for the electrochemical determination of Cu, Cd and Mn using differential pulse stripping voltammetry (DPSV). The voltammograms were probed using a cell and three electrodes. Ag/AgCl/KCl (2.0 mol L^{-1}), $NiFe_2O_4 \cdot CoFe_2O_4$-NC/GCE, and a Pt wire were used as the reference, working, and auxiliary electrodes, respectively. During the analysis, the target metal ions were pre-concentrated at a potential of −1.6 V for 2.0 min, followed by anodic stripping within the potential range of −0.8 to 0.0 V. The DPSV measurements were conducted under optimized conditions, with pulse amplitude of 0.05 V, pulse period of 0.5 s, pulse width of 0.05 s, and sampling time of 0.0167 s.

2.6 Instrumentation

The $NiFe_2O_4 \cdot CoFe_2O_4$-NC is characterized using various analytical techniques to determine its structural, morphological and electrochemical properties. X-ray diffraction (XRD) and atomic force microscopy (AFM) analyses were carried out using

D-8 and Nano-Scope V instruments (Bruker) to evaluate the crystal structure and particle size distribution. The surface morphology and elemental composition were examined using scanning electron microscopy (SEM) and energy-dispersive X-ray spectroscopy (EDX) with JEOL JSM-7600F (Japan).

Differential pulse stripping voltammetry (DPSV) was conducted using a CHI820D electrochemical analyzer (Austin, USA), employing a conventional three electrode configuration consisting of an Ag/AgCl reference electrode, platinum (Pt) wire counter electrode, and a $NiFe_2O_4 \cdot CoFe_2O_4$-NC/GCE working electrode. The zeta potential (ZP) and hydrodynamic size of the $NiFe_2O_4 \cdot CoFe_2O_4$-NC is determined using a zeta potential analyzer and a dynamic light scattering (DLS) system (ELSZ-2000).

3 Results and discussion

3.1 Characterization

The XRD technique was used to study the structure, size and crystallinity of synthesized materials, and the results are shown in Fig. 1a. In the XRD spectrum of $NiFe_2O_4$-NPs, the most powerful diffraction peak at $2\Theta = 35.6$ and plane spacing $d = 2.494$ Å corresponds to the (311) plane of $NiFe_2O_4$-NPs.[31] According to the standard of JCPDS (Card No. 10-0325), the $NiFe_2O_4$-NPs can be categorized as spinel and face-centred cubic (fcc) structures.[32] No diffraction peaks of other impurities are perceived. The Debye–Scherrer equation was useful in defining the average size of synthesized $NiFe_2O_4$-NPs and the average size was found to be 11.21 nm.[33] The sharpness of peaks shows a higher degree of crystallinity, and the % crystallinity of $NiFe_2O_4$-NPs was found to be 77%.[21] Similarly, the XRD patterns of $CoFe_2O_4$-NPs show that all the peaks relate to the characteristic peaks of the cubic spinel lattice of $CoFe_2O_4$ (JCPDS File No. 22-1086), indicating that the samples have a single-phase spinel structure. The Debye–Scherrer equation was applied to determine the average size of synthesized $CoFe_2O_4$-NPs and the average size was found 7.78 nm.[33] The quickness of peaks shows a higher degree of crystallinity and the % crystallinity of $CoFe_2O_4$-NPs was found 79%.[21] Additional, diffraction peaks at 2Θ values of 30.7, 35.9, 37.4, 43.6, 57.6, 63.1 resemble to the crystal planes (220), (311), (222), (400), (422), (511), (440), correspondingly and one additional peak was detected as an

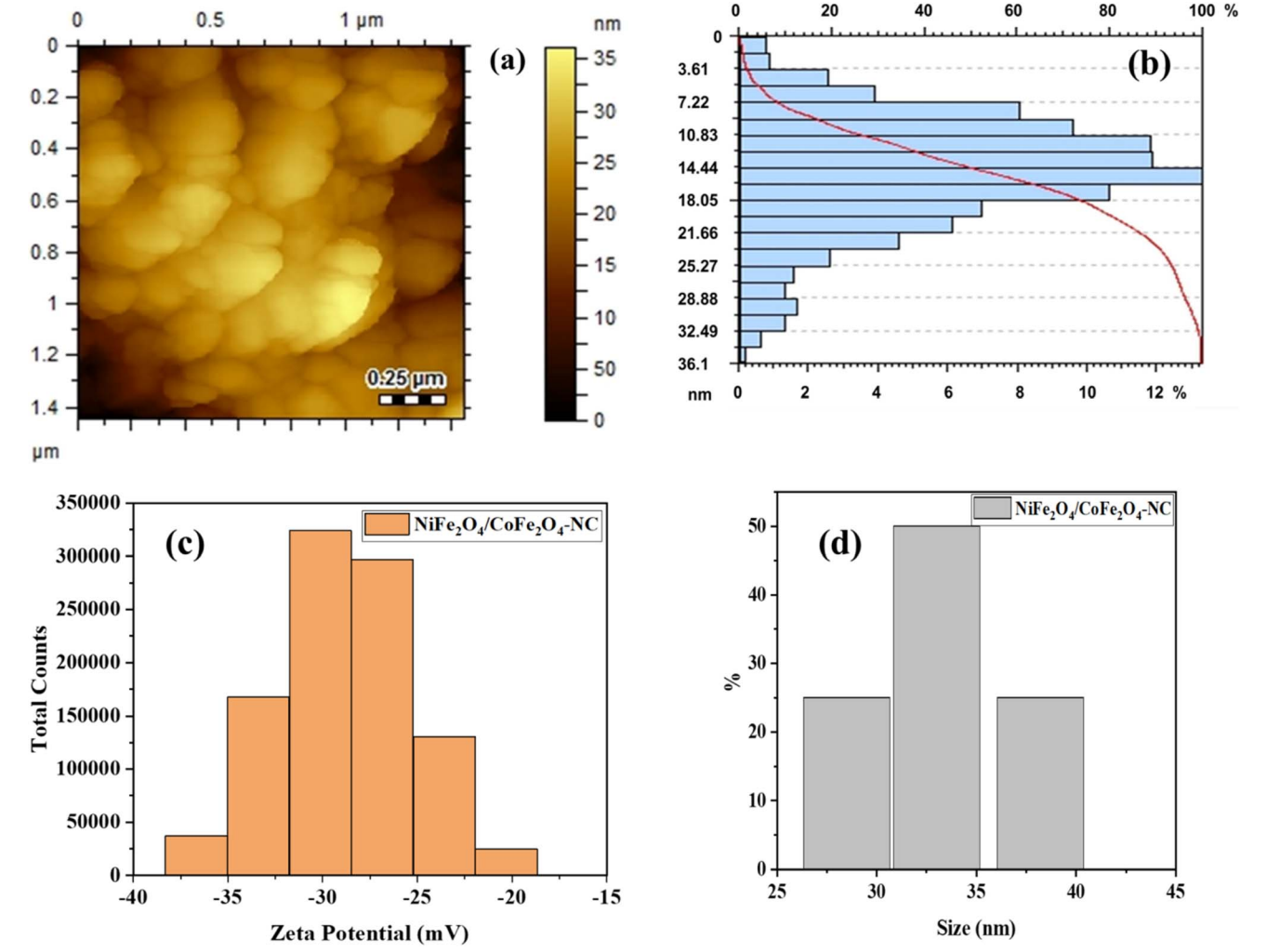

Fig. 2 (a) Surface topography and (b) bar graph study of $NiFe_2O_4 \cdot CoFe_2O_4$-NC using AFM, (c) zeta potential, and (d) hydrodynamic size of $NiFe_2O_4 \cdot CoFe_2O_4$-NC.

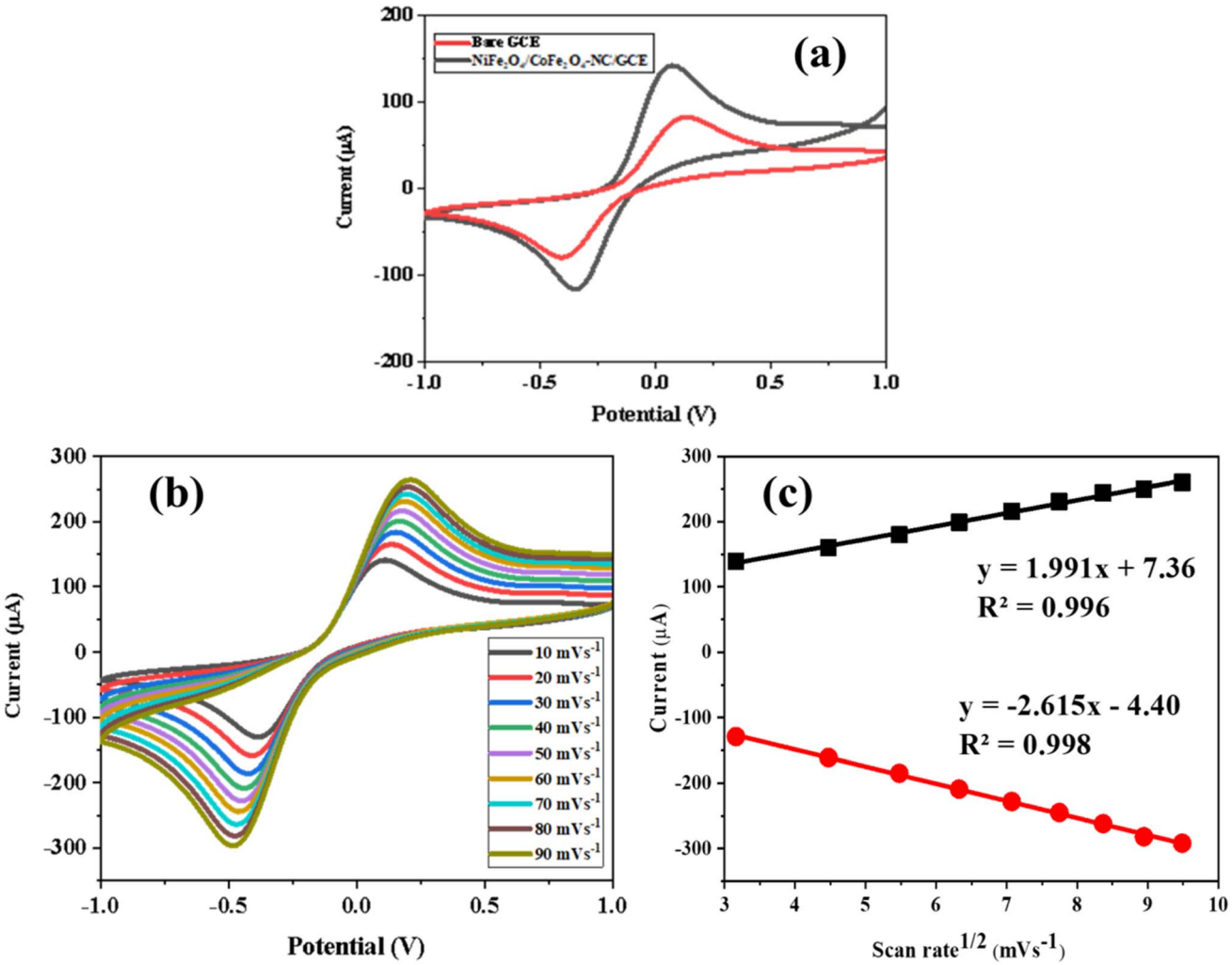

Fig. 3 (a) Optimization of sensitivity of bare and $NiFe_2O_4 \cdot CoFe_2O_4$-NC/GCE and (b) scan rate study and (c) linear relationship of current *vs.* square root of scan rate of $NiFe_2O_4 \cdot CoFe_2O_4$-NC/GCE.

impurity may be due to formation of α-Fe_2O_3 at 34.2 which corresponds to 104 (JCPDS No. 33-0664).[34] The diffraction peak patterns of $NiFe_2O_4 \cdot CoFe_2O_4$-NC expose that all the peaks correspond to the characteristic peaks of the spinel lattice of $NiFe_2O_4 \cdot CoFe_2O_4$-NC.[35] The Debye–Scherrer equation was useful in defining the average size of synthesized $NiFe_2O_4 \cdot CoFe_2O_4$-NC, and the average size was found to be 23.11 nm.[33] The sharpness of peaks shows a higher degree of crystallinity, and the % crystallinity of $NiFe_2O_4 \cdot CoFe_2O_4$-NC was found to be 96%.[21]

Further, the SEM analysis is carried out to study the surface morphology. The SEM results are shown in Fig. 1(b), which demonstrates the porosity of $NiFe_2O_4 \cdot CoFe_2O_4$-NC with a rough and uniform surface.

Moreover, the purity of synthesized $NiFe_2O_4 \cdot CoFe_2O_4$-NC is also studied by analyzing its elemental composition using EDX. The results of elemental composition are provided in Fig. 1 (c), which shows the presence of cobalt (Co), nickel (Ni), iron (Fe) and oxygen (O) at 6.1, 14.4, 29.3 and 50.1%, respectively. The presence of these elements confirms the successful synthesis of the $NiFe_2O_4 \cdot CoFe_2O_4$-NC, and it also confirms the purity of synthesized material.

The surface structure and size distribution of $NiFe_2O_4 \cdot CoFe_2O_4$-NC were considered using the AFM technique. The two-dimensional image of AFM showed that the $NiFe_2O_4 \cdot CoFe_2O_4$-NC had seemed to merge (Fig. 2a). The $NiFe_2O_4 \cdot CoFe_2O_4$-NC present a plane surface that may be understood to point out that it had an identical attachments without significant disturbances.[36] Further, the size of the $NiFe_2O_4 \cdot CoFe_2O_4$-NC was also studied from AFM bar graph which showed the size distribution in the range of 1.5 to 36.1 nm with an average particle size of 15.7 nm (Fig. 2b).

The ZP is studied to confirm surface charge of $NiFe_2O_4 \cdot CoFe_2O_4$-NC in aqueous solution. Typically, a ZP value $>\pm 30$ mV shows repulsive forces that prevent the aggregation of the particles. Fig. 2(c) shows that the average ZP of synthesized $NiFe_2O_4 \cdot CoFe_2O_4$-NC is -34.53 ± 9.9 mV, which confirms excellent stability of nanocomposite. Furthermore, the average hydrodynamic size of $NiFe_2O_4 \cdot CoFe_2O_4$-NC is determined to be 32.0 ± 5.43 nm (Fig. 2d).

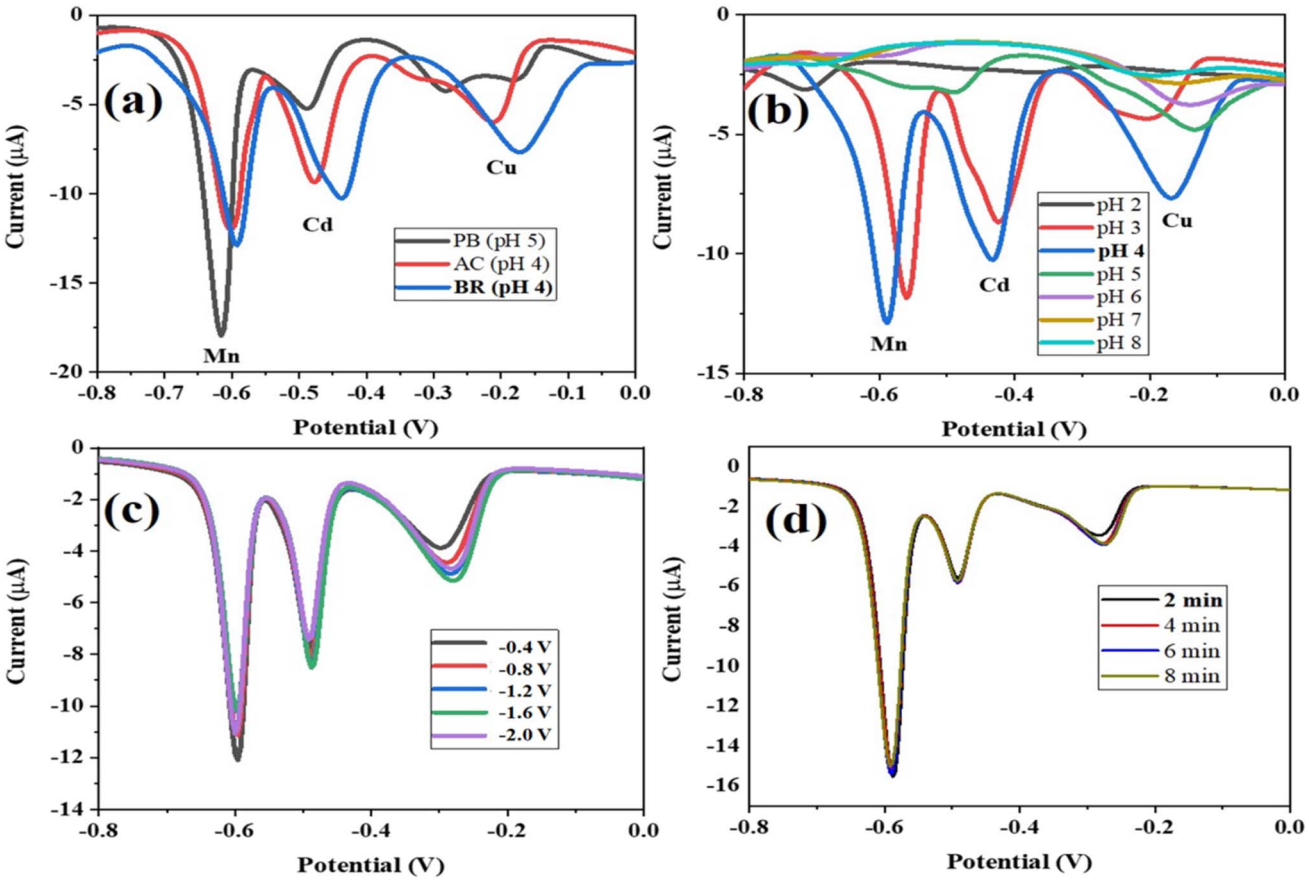

Fig. 4 Optimization of (a) electrolyte, (b) pH, (c) deposition potential and (d) deposition time of $NiFe_2O_4 \cdot CoFe_2O_4$-NC/GCE for the detection of Cd, Cu and Mn.

3.2 Electrochemical studies

The electrochemical performance of both of bare GCE and $NiFe_2O_4 \cdot CoFe_2O_4$-NC/GCE are evaluated by cyclic voltammetry (CV) in the solution $[Fe(CN)_6]^{4-}$ (5.0 mM) and KCl (100 mM) as supporting electrolyte (Fig. 3a). The CV results revealed that both electrodes exhibited redox current responses, with the $NiFe_2O_4 \cdot CoFe_2O_4$-NC/GCE showing the highier response. This enhancement is attributed to the larger electroactive surface area of the $NiFe_2O_4 \cdot CoFe_2O_4$-NC/GCE.[33] Therefore, $NiFe_2O_4 \cdot CoFe_2O_4$-NC/GCE is selected for further electrochemical investigations.

The electron transfer kinetics of $NiFe_2O_4 \cdot CoFe_2O_4$-NC/GCE is further examined through CV at varying scan rates ranging from 10 to 90 mV s^{-1} in the same electrolyte (Fig. 3b). An increase in the scan rate resulted in a proportional rise in redox peak currents, suggesting that the electrochemical process is diffusion controlled. The higher scan rates reduce reaction time, reducing the diffusion layer and allowing a greater number of electroactive species to reach the electrode surface.[30,37] A linear relationship (with $R^2 > 0.998$) was observed between the peak current and the square root of the scan rate (Fig. 3c), confirming that the redox process at the $NiFe_2O_4 \cdot CoFe_2O_4$-NC/GCE is followed diffusion controlled kinetics.

After successful electrochemical characterization of $NiFe_2O_4 \cdot CoFe_2O_4$-NC/GCE. various experimental parameters, including supporting electrolyte, pH, deposition potential, and deposition time, were optimized to enhance electrochemical performance. The effect of different electrolytes Britton Robinson (BR) buffer, phosphate buffer (PB), and acetic acid/sodium acetate (NaAc/HAc; AC) are evaluated (Fig. 4a). Among these, the BR buffer exhibited the highest and most stable current response, therefore, it was selected as the optimal supporting electrolyte for subsequent electrochemical studies.

The effect of pH on electrochemical detection of Cd, Cu and Mn was examined using BR buffer (0.1 M) within the pH range of 2.0–8.0 (Fig. 4b). The results showed that the peak current increased with rising pH up to 4.0, after which it declined, likely due to the presence of oxygen containing functional groups on the $NiFe_2O_4 \cdot CoFe_2O_4$-NC surface.[38] At lower pH levels (pH < 4.0), $NiFe_2O_4 \cdot CoFe_2O_4$-NC become protonated, competing with metal ions for active binding sites and disrupting electrostatic interactions with Cd, Cu, and Mn. Conversely, the decrease in current at higher pH values (pH > 4.0) may be attributed to the hydrolysis of metal ions, reducing their availability for electrochemical interaction.[30,39] Therefore, pH 4.0 was selected as the optimal condition for subsequent analyses. Notably, the Mn^{2+} reduction peak was observed at −0.6 V, which is more negative than values commonly reported for unmodified electrodes. This shift arises from the use of the $NiFe_2O_4 \cdot CoFe_2O_4$-NC/GCE, which affects electron-transfer kinetics and surface adsorption

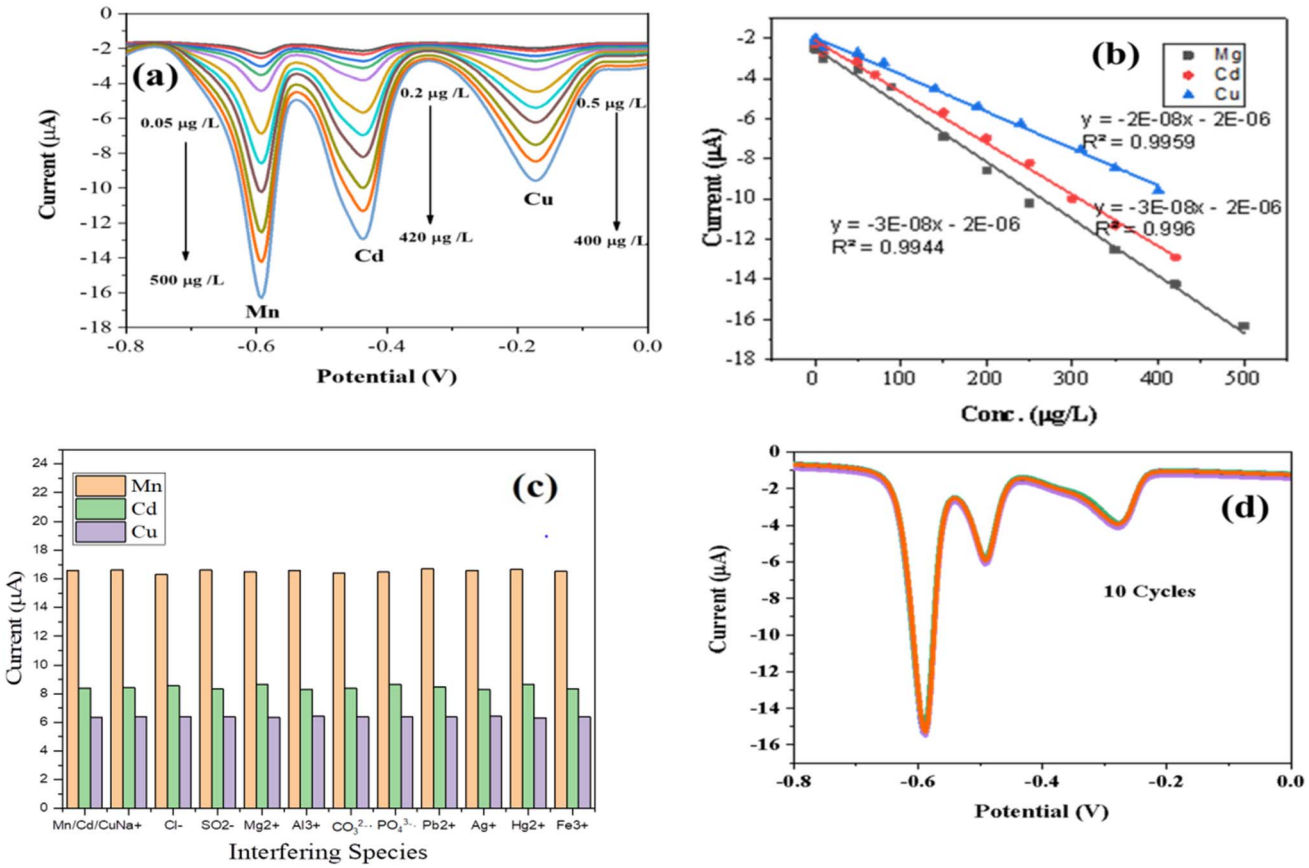

Fig. 5 (a) Calibration, (b) linear relationship between current and concentration, (c) interference and stability analysis of $NiFe_2O_4 \cdot CoFe_2O_4$-NC/GCE for the detection of Cd, Cu and Mn, and (d) stability of $NiFe_2O_4 \cdot CoFe_2O_4$-NC/GCE for simultaneous electrochemical detection of Cd, Cu, and Mn.

properties. Additionally, the supporting electrolyte composition and pH influence the reduction potential, leading to a more cathodic peak compared to literature values obtained on bare or differently modified electrodes.

The influence of deposition potential on the simultaneous detection of Cd, Cu and Mn was examined within the range of −0.4 to −2.0 V (Fig. 4c). The highest current response for all three metals was obtained at 60 mV, indicating that this potential provided the greatest detection efficiency of the $NiFe_2O_4 \cdot CoFe_2O_4$-NC/GCE. Selecting a low deposition potential is crucial due to the standard reduction potentials of Cd^{2+}/Cd ($E° = -0.402$ V), Cu^{2+}/Cu ($E° = +0.340$ V), and Mn^{2+}/Mn ($E° = -1.18$ V). For Cd^{2+} and Mn^{2+}, which possess more negative reduction potentials, operating at −1.6 V ensures effective reduction and pre-concentration without triggering hydrogen evolution that typically occurs at more negative potentials. Although Cu^{2+} has a more positive reduction potential, efficient deposition at −1.6 V is attributed to the catalytic activity of the $NiFe_2O_4 \cdot CoFe_2O_4$-NC/GCE. Thus, applying −1.6 V allows efficient reduction and accumulation of Cd, Cu, and Mn while minimizing interference from hydrogen evolution.[40] Additionally, this potential enhances selectivity by favoring the reduction of the target metals over other competing ions, ensuring precise and reliable detection.[41] Consequently, −1.6 V was selected as the optimal deposition potential for further electrochemical analyses.

The effect of deposition time was also evaluated in the range of 2–8 min for the simultaneous detection of Cd, Cu, and Mn. The negligible increase in current response is observed with longer deposition times. However, after 8 min, no significant improvement was observed (Fig. 4d). Therefore, a deposition time of 2 min was identified as optimal for subsequent electrochemical measurements.

The performance of the $NiFe_2O_4 \cdot CoFe_2O_4$-NC/GCE is evaluated for the simultaneous detection of Cd, Cu, and Mn over concentration ranges of 0.2–420 µg L^{-1}, 0.5–400 µg L^{-1}, and 0.05–500 µg L^{-1}, respectively, using differential pulse voltammetry (DPV) (Fig. 5a and b). A linear relationship was observed between the peak current response and the concentration of each metal ion. The limits of detection and quantification (LOD and LOQ) are calculated 0.083 µg L^{-1} and 0.25 µg L^{-1} for Cd, 0.188 µg L^{-1} and 0.57 µg L^{-1} for Cu, and 0.026 µg L^{-1} and 0.08 µg L^{-1} for Mn. The LOD and LOQ was calculated by using formulas as "3.3 (Standard deviation of intercept of calibration curve)/Slope" and "10 (Standard deviation of intercept of calibration curve)/Slope", respectively.[42,43] These results demonstrate that the $NiFe_2O_4 \cdot CoFe_2O_4$-NC/GCE provides effective and simultaneous detection of Cd, Cu, and Mn, making it highly suitable for the analysis of environmental samples.

Table 1 Simultaneous determination of Cd, Cu and Mn in real samples by developed electrochemical method

Sample	Analyte	Added ($\mu g\ L^{-1}$)	Found ($\mu g\ L^{-1}$)	Recovery (%)	RSD (%)
Tap water	Cd	0.00	6.42	—	1.56
		100	97.1	97.1	1.64
		200	197	98.8	1.52
	Cu	0.00	374	—	2.07
		100	96.4	96.4	1.72
		200	195	97.7	1.46
	Mn	0.00	182	—	1.69
		100	96.8	96.8	1.53
		200	196	97.9	1.44
Milk	Cd	0.00	0.217	—	2.71
		100	92.8	92.8	3.24
		200	184	92.1	2.48
	Cu	0.00	253	—	2.91
		100	96.7	96.7	2.46
		200	192	95.7	1.93
	Mn	0.00	163	—	2.68
		100	96.6	96.6	2.93
		200	192	96.2	2.71
Mango juice	Cd	0.00	5.09	—	1.97
		100	94.9	94.9	3.02
		200	196	98.1	2.76
	Cu	0.00	14.2	—	2.38
		100	95.7	95.7	2.34
		200	197.5	98.8	2.95
	Mn	0.00	3.21	—	3.42
		100	96.9	96.9	2.62
		200	197	98.6	2.19

The selectivity of $NiFe_2O_4 \cdot CoFe_2O_4$-NC/GCE is evaluated by introducing eight possible interfering ions (Pb^{2+}, Ag^{+}, Hg^{2+}, and Fe^{3+}, Na^{+}, Cl^{-}, SO_4^{2-}, Mg^{2+}, Al^{3+}, CO_3^{2-}, and PO_4^{3-}) into the analyte (Cd, Cu and Mn). These interfering ions were present at concentrations 5 times higher than those of the target metals. The results revealed that the presence of these ions had no significant impact on the simultaneous detection of Cd, Cu, and Mn (Fig. 5c). This demonstrates that the $NiFe_2O_4 \cdot CoFe_2O_4$-NC/GCE possesses strong selectivity and can accurately detect these metals in real samples.

The stability $NiFe_2O_4 \cdot CoFe_2O_4$-NC/GCE is further examined through ten repeated DPV measurements taken at different time intervals, which showed consistent current responses with a relative standard deviation (RSD) of 2.84% (Fig. 5d). These results confirm the excellent stability and reusability of the $NiFe_2O_4 \cdot CoFe_2O_4$-NC/GCE for simultaneous electrocatalytic detection of Cd, Cu, and Mn. Furthermore, the reproducibility of fabricated sensor was also studied by synthesizing four new electrodes by identical method. The current responses of all the newly fabricated sensors were very close to each other with RSD of less than 5%. These results indicated that the fabrication method is reproducible and can be successfully applied for the routine analysis TMS.

To validate its practical application, the developed $NiFe_2O_4 \cdot CoFe_2O_4$-NC/GCE based method was applied to tap water, mango juice, and milk samples collected from the local market in Jamshoro, Sindh, Pakistan. Tap water and juice samples were filtered and centrifuged to remove suspended particles. Milk sample are filtered to remove the solid impurities and analyzed by voltammetry for the detection selected metals. The concentrations of Cd, Cu, and Mn are found 6.42, 374, and 182 $\mu g\ L^{-1}$ in tap water, 0.217, 253, and 163 $\mu g\ L^{-1}$ in milk, and 5.09, 14.2, and 3.21 $\mu g\ L^{-1}$ in juice samples respectively. Moreover the standard addition method was employed to verify the accuracy and reliability of the developed approach, and the corresponding results are presented in Table 1. The high recovery values ranging from 92.1% to 98.8% for the simultaneous determination of Cd, Cu, and Mn, with RSD of less than 4%, demonstrate that the developed method is reliable, and suitable for real sample analysis of these metals.

The analytical performance of the proposed voltammetric method using $NiFe_2O_4 \cdot CoFe_2O_4$-NC/GCE for detecting Cd, Cu, and Mn was compared with previously reported techniques. The comparison (Table 2) reveals that the $NiFe_2O_4 \cdot CoFe_2O_4$-NC/GCE based method offers a wider concentration range and

Table 2 Comparative study of current work with reported methods for the detection of Cd, Cu and Mn[a]

Electrodes	Technique	Analyte	Linear range ($\mu g\ L^{-1}$)	LOD ($\mu g\ L^{-1}$)	References
PPE/GCE	SWASV	Cd	2.0–100.0	0.8	44
Bi@BAC/CPE	DPASV	Cd	4.5–446.4	0.7	45
PPy/graphene/Au	SWASV	Cd	8.9–89.3	0.45	46
AuNPs/SPGE	DPASV	Cu	20 – 300	1.6	47
Au SPGE-LT	SWASV	Cu	5–300	1.5	48
AuNPs SPCE arrays	SWASV	Cu	10–150	1.4	49
Edge plane pyrolytic graphite electrode	SWASV	Mn	0.62–174	0.3	50
Modified bentonite–porphyrin carbon paste electrode	SWASV	Mn	0.6–500	0.1	51
Metal catalyst free carbon nanotube (MCFCNT)	SWASV	Mn	0.6–6.7	0.093	52
$NiFe_2O_4 \cdot CoFe_2O_4$/GCE	DPV	Cd	0.05–500	0.083	Current study
		Cu	0.2–400	0.188	
		Mn	0.5–400	0.026	

[a] PPE/GCE; 1-phenyl-*N*-(pyridin-2-ylmethyl)ethanamine based glassy carbon electrode, Bi@BAC/CPE; bismuth/biomass derived activated carbon, PPy/graphene/Au; porous graphene oxide-polypyrrole (pGO/PPy) polymer nanocomposite, AuNPs/SPGE; screen-printed gold electrode with gold nanoparticles, Au SPGE-LT; low temperature gold-cured screen-printed electrode, AuNPs SPCE arrays; gold nanoparticles screen-printed carbon electrode arrays, edge plane pyrolytic graphite electrode; edge plane pyrolytic graphite electrode, MBPCE; modified bentonite porphyrin carbon paste electrode, MBPCE; modified bentonite–porphyrin carbon paste electrode, MCFCNT; metal catalyst free carbon nanotube.

lower detection limits than those achieved in earlier studies, demonstrating its superior analytical efficiency. Improved electron transfer efficiency reduces the charge transfer resistance during the redox reactions of Cd, Cu, and Mn, thereby enhancing the electrode's catalytic performance. The outstanding electrochemical behavior of $NiFe_2O_4 \cdot CoFe_2O_4$-NC/GCE can also be attributed to the effective synthesis of the nanocomposite. Comparison with previously reported Cd, Cu, and Mn detection methods further validates the reliability and effectiveness of the developed approach.

4 Conclusion

The $NiFe_2O_4 \cdot CoFe_2O_4$ nanocomposite was employed for the determination of Cd, Cu and Mn based on the modified GCE. Incorporating $NiFe_2O_4 \cdot CoFe_2O_4$-NC onto the GCE significantly enhanced the oxidation peak current, sensitivity, and sharpness while reducing the overpotential for Cd, Cu, and Mn oxidation. These improvements can be attributed to the strong and efficient interaction between the analytes and the metallic sites on the $NiFe_2O_4 \cdot CoFe_2O_4$-NC surface. The large active surface area, excellent adsorption capacity, and selective interaction properties of the nanocomposite contribute to its high detection efficiency. Compared to previously reported sensors, the developed electrode offers several advantages, including an exceptionally low detection limit, broad linear range, high sensitivity, strong stability, excellent repeatability and reproducibility, and a straightforward modification process for detecting Cd, Cu, and Mn in tap water, mango juice, and milk samples.

Ethical statement

The current experimental investigations do not contain any kind of involvement either direct or indirect of human contributors and animals.

Author contributions

Hassan Imran Afridi and Jameel Ahmed Baig; conceptualization, supervision, writing and editing, formal analysis, methodology, and resources. Zahid Ali, Khalil Akhtar, Saima Perveen, and Nadeem Raza; methodology, writing, editing, visualization.

Conflicts of interest

The authors declare that they have no known competing financial interests or personal relationships that could have appeared to influence the work reported in this paper.

Data availability

Access to the data assisting with the current research project can be granted upon formal request.

Acknowledgements

This work was supported and funded by the Deanship of Scientific Research at Imam Mohammad Ibn Saud Islamic University (IMSIU) (grant number IMSIU-DDRSP2502).

References

1 D. Li, J. Yin, Z. Yu, Z. Gao, N. Xu and L. Meng, Artificial intelligence-assisted colorimetric sensor array based on supramolecular self-assembled nanozymes for visual monitoring of pesticide residues, *Sens. Actuators, B*, 2025, 138493.
2 Y. Li, Y. Zhou, X. Liu, J. Lei, X. Qin, G. Li and Z. Yang, A NIR ratiometric fluorescence probe for rapid, sensitive detection and bioimaging of hypochlorous acid, *Spectrochim. Acta, Part A*, 2023, **302**, 123102.
3 P. O. Ukaogo, U. Ewuzie and C. V. Onwuka, "Environmental pollution: causes, effects, and the remedies", in *Microorganisms for Sustainable Environment and Health*, Elsevier, 2020, pp. 419–429.
4 C. D. Klaassen, J. Liu and B. A. Diwan, Metallothionein protection of cadmium toxicity, *Toxicol. Appl. Pharmacol.*, 2009, **238**, 215–220.
5 Y.-S. Lin, J. L. Caffrey, J.-W. Lin, D. Bayliss, M. F. Faramawi, T. F. Bateson and B. Sonawane, Increased risk of cancer mortality associated with cadmium exposures in older Americans with low zinc intake, *J. Toxicol. Environ. Health, Part A*, 2013, **76**, 1–15.
6 L. Zhao, M. Liao, L. Li, L. Chen, T. Zhang and R. Li, Cadmium activates the innate immune system through the AIM2 inflammasome, *Chem.-Biol. Interact.*, 2024, **399**, 111122.
7 M. Azizur Rahman, M. M. Rahman, S. M. Reichman, R. P. Lim and R. Naidu, Heavy metals in Australian grown and imported rice and vegetables on sale in Australia: Health hazard, *Ecotoxicol. Environ. Saf.*, 2014, **100**, 53–60.
8 M. Harmanescu, L. M. Alda, D. M. Bordean, I. Gogoasa and I. J. Gergen, Heavy metals health risk assessment for population via consumption of vegetables grown in old mining area; a case study: Banat County, Romania, *Chem. Cent. J.*, 2011, **5**, 64.
9 Z. Jia, S. Li and L. Wang, Assessment of soil heavy metals for eco-environment and human health in a rapidly urbanization area of the upper Yangtze Basin, *Sci. Rep.*, 2018, **8**, 3256.
10 J. Baj, W. Flieger, A. Barbachowska, B. Kowalska, M. Flieger, A. Forma, G. Teresiński, P. Portincasa, G. Buszewicz and E. Radzikowska-Büchner, Consequences of disturbing manganese homeostasis, *Int. J. Mol. Sci.*, 2023, **24**, 14959.
11 R. S. Fernandes and N. Dey, Ion-specific bathochromic shifts: Simultaneous detection of multiple heavy metal pollutants via charge transfer interactions, *J. Mol. Liq.*, 2022, **367**, 120369.
12 K. Kannan, J. Mukherjee, P. Mishra and M. N. Gupta, Nickel ferrite nanoparticles as an adsorbent for immobilized metal affinity chromatography of proteins, *J. Chromatogr. Sci.*, 2021, **59**, 262–268.

13 M. Wu, B. Yang, L. Shi, Q. Tang, J. Wang, W. Liu, B. Li and Y. Jin, Peroxidase-mimicking DNAzymes as receptors for label-free discriminating heavy metal ions by chemiluminescence sensor arrays, *Anal. Chem.*, 2023, **95**, 3486–3492.

14 E. Al-Hetlani, M. O. Amin, M. Madkour and B. D'Cruz, Forensic determination of pesticides in human serum using metal ferrites nanoparticles and SALDI-MS, *Talanta*, 2021, **221**, 121556.

15 J. Nayak, S. K. Sahoo and R. Kumar, Study of anticancer drugs interaction with hemoglobin by electrochemical methods and molecular docking: implications towards anticancer treatment, *ChemistrySelect*, 2021, **6**, 4098–4106.

16 N. An, T. Chen, J. Zhang, G. Wang, M. Yan and S. Yang, Rational electrochemical design of cuprous oxide hierarchical microarchitectures and their derivatives for SERS sensing applications, *Small Methods*, 2024, **8**, 2300910.

17 L. Xie, L. Liu, S. Xu, T. Wang, X. Yue and G. Li, An efficient voltammetric sensing platform for trace determination of Norfloxacin based on nanoplate-like α-zirconium phosphate/carboxylated multiwalled carbon nanotube nanocomposites, *Microchem. J.*, 2024, **206**, 111451.

18 F. Qian, R. Jia, M. Cheng, A. Chaudhary, S. Melhi, S. D. Mekkey, N. Zhu, C. Wang, F. Razak and X. Xu, An overview of polylactic acid (PLA) nanocomposites for sensors, *Adv. Compos. Hybrid Mater.*, 2024, **7**, 75.

19 A. Hojjati-Najafabadi, S. Salmanpour, F. Sen, P. N. Asrami, M. Mahdavian and M. A. Khalilzadeh, A tramadol drug electrochemical sensor amplified by biosynthesized Au nanoparticle using mentha aquatic extract and ionic liquid, *Top. Catal.*, 2022, **65**, 587–594.

20 S. Perveen, J. A. Baig, M. Nur-e-Alam, M. Kazi, S. Memon, T. G. Kazi, K. Akhtar and S. Hussain, Electrocatalytic detection of Acetaminophen by sodium ferrite, *Results Phys.*, 2025, **68**, 108073.

21 S. Perveen, J. A. Baig, S. T. H. Sherazi, S. Memon, K. Akhtar, S. Hussain and F. Abbasi, Green Synthesis of Electroactive Magnesium Ferrite Nanoparticles for the Selective Determination of Mefenamic Acid in Blood, Pharmaceutical Products, and Wastewater, *Anal. Lett.*, 2024, 1–16.

22 B. Muthukutty, J. Ganesamurthi, S.-M. Chen, B. Arumugam, S. M. Wabaidur, Z. A. ALOthman, T. Altalhi and M. A. Ali, Construction of novel binary metal oxides: Copper oxide–tin oxide nanoparticles regulated for selective and nanomolar level electrochemical detection of anti-psychotic drug, *Electrochim. Acta*, 2021, **386**, 138482.

23 N. T. Anh, N. Van Quy, O. Van Hoang, N. X. Dinh and A.-T. Le, An on-site and portable electrochemical sensing platform based on spinel zinc ferrite nanoparticles for the quality control of paracetamol in pharmaceutical samples, *Nanoscale Adv.*, 2024, **6**, 256–267.

24 V. Sanko, A. Şenocak, S. O. Tümay and E. Demirbas, A novel comparative study for electrochemical urea biosensor design: Effect of different ferrite nanoparticles (MFe2O4, M: Cu, Co, Ni, Zn) in urease immobilized composite system, *Bioelectrochemistry*, 2023, **149**, 108324.

25 A. Tripathy, M. J. Nine and F. S. Silva, Biosensing platform on ferrite magnetic nanoparticles: Synthesis, functionalization, mechanism and applications, *Adv. Colloid Interface Sci.*, 2021, **290**, 102380.

26 H. Zhang, L. Li, C. Wang, Q. Liu, W.-T. Chen, S. Gao and G. Hu, Recent advances in designable nanomaterial-based electrochemical sensors for environmental heavy-metal detection, *Nanoscale*, 2025, 2386–2407.

27 F. Abbasi, I. B. Solangi, J. A. Baig, S. Hussain, S. Perveen, K. Akhtar, S. A. Solangi and P. Bhanbhro, Innovative approach for trace level detection of mefenamic acid by ferrite nanocomposite-based electrochemical sensor, *Mater. Today Commun.*, 2024, **40**, 109739.

28 M. Tulinski and M. J. M. Jurczyk, *Nanomaterials Synthesis Methods: Protocols and Industrial Innovations*, 2017, pp. 75–98.

29 K. Akhtar, J. A. Baig, S. A. Solangi, S. Perveen, S. Hussain, T. G. Kazi, H. I. Afridi and F. Abbasi, Phytoextract based synthesis of TiO2. Al2O3 nanocomposites for efficient electrocatalytic detection of acetaminophen from environmental and pharmaceutical samples, *Ceram. Int.*, 2024, **50**, 11012–11021.

30 S. Perveen, J. A. Baig, S. T. H. Sherazi, H. I. Afridi, E. Fricovsky, S. Sanam and K. Akhtar, Graphene oxide/magnesium ferrite nanocomposite modified electrochemical sensor for simultaneous detection of cadmium and lead, *Microchem. J.*, 2025, 114148.

31 S. Maensiri, C. Masingboon, B. Boonchom and S. Seraphin, A simple route to synthesize nickel ferrite (NiFe2O4) nanoparticles using egg white, *Scr. Mater.*, 2007, **56**, 797–800.

32 S. Qu, J. Wang, J. Kong, P. Yang and G. Chen, Magnetic loading of carbon nanotube/nano-Fe3O4 composite for electrochemical sensing, *Talanta*, 2007, **71**, 1096–1102.

33 P. K. Kannan, S. A. Moshkalev and C. S. Rout, Electrochemical sensing of hydrazine using multilayer graphene nanobelts, *RSC Adv.*, 2016, **6**, 11329–11334.

34 F. Wang, X. Qin, Y. Meng, Z. Guo, L. Yang and Y. J. Ming, Hydrothermal synthesis and characterization of α-Fe2O3 nanoparticles, *Mater. Sci. Semicond. Process.*, 2013, **16**, 802–806.

35 K. Nejati and R. Zabihi, Preparation and magnetic properties of nano size nickel ferrite particles using hydrothermal method, *Chem. Cent. J.*, 2012, **6**, 1–6.

36 D. Hassan, A. Sani, A. Antonio Pérez, M. Ehsan, J. D. Hernández-Varela, J. J. Chanona-Pérez and A. L. Torres Huerta, The Impact of Nickel–Zinc Ferrite Nanoparticles on the Mechanical and Barrier Properties of Green-Synthesized Chitosan Films Produced Using Natural Juices, *Polymers*, 2024, **16**, 3455.

37 N. P. Godman, J. L. DeLuca, S. R. McCollum, D. W. Schmidtke and D. T. Glatzhofer, Electrochemical characterization of layer-by-layer assembled ferrocene-modified linear poly (ethylenimine)/enzyme bioanodes for glucose sensor and biofuel cell applications, *Langmuir*, 2016, **32**, 3541–3551.

38 B. Wang, J. Chen, H. Tong, Y. Huang, B. Liu, X. Yang, Z. Su, X. Tu and X. Qin, Simultaneous electrochemical detection of

Cd (II) and Pb (II) based on L-cysteine functionalized gold nanoparticles/metal-organic frameworks-graphene oxide nanocomposites, *J. Electroanal. Chem.*, 2023, **943**, 117573.

39 J. Huang, F. Yuan, G. Zeng, X. Li, Y. Gu, L. Shi, W. Liu and Y. Shi, Influence of pH on heavy metal speciation and removal from wastewater using micellar-enhanced ultrafiltration, *Chemosphere*, 2017, **173**, 199–206.

40 C. M. Welch and R. G. Compton, The use of nanoparticles in electroanalysis: a review, *Anal. Bioanal. Chem.*, 2006, **384**, 601–619.

41 M. Fayazi, M. Ghanei-Motlagh and C. Karami, Application of magnetic nanoparticles modified with L-cysteine for pre-concentration and voltammetric detection of copper (II), *Microchem. J.*, 2022, **181**, 107652.

42 S. Perveen, A. Hol, J. A. Baig, S. T. H. Sherazi, K. Akhtar, S. Hussain and F. Abbasi, Sodium nanoferrite-based solid phase extraction: a green method for the simultaneous determination of cadmium, copper, and lead, *J. Anal. At. Spectrom.*, 2024, **39**, 2884–2892.

43 M. M. El-Wekil, H. R. H. Ali, A. A. Marzouk and R. Ali, Enhanced dispersive solid phase extraction assisted by cloud point strategy prior to fluorometric determination of anti-hepatitis C drug velpatasvir in pharmaceutical tablets and body fluids, *RSC Adv.*, 2018, **8**, 13292–13300.

44 A. Shah, S. Sultan, A. Zahid, S. Aftab, J. Nisar, S. Nayab, R. Qureshi, G. S. Khan, H. Hussain and S. A. Ozkan, Highly sensitive and selective electrochemical sensor for the trace level detection of mercury and cadmium, *Electrochim. Acta*, 2017, **258**, 1397–1403.

45 X. Zhu, B. Liu, S. Chen, L. Wu, J. Yang, S. Liang, K. Xiao, J. Hu and H. Hou, Ultrasensitive and simultaneous electrochemical determination of Pb2+ and Cd2+ based on biomass derived lotus root-like hierarchical porous carbon/bismuth composite, *J. Electrochem. Soc.*, 2020, **167**, 087505.

46 Y. Song, C. Bian, J. Hu, Y. Li, J. Tong, J. Sun, G. Gao and S. Xia, Porous polypyrrole/graphene oxide functionalized with carboxyl composite for electrochemical sensor of trace cadmium (II), *J. Electrochem. Soc.*, 2019, **166**, B95.

47 N. M. Thanh, N. Van Hop, N. D. Luyen, N. H. Phong and T. T. Tam Toan, Simultaneous Determination of Zn (II), Cd (II), Pb (II), and Cu (II) Using Differential Pulse Anodic Stripping Voltammetry at a Bismuth Film-Modified Electrode, *Adv. Mater. Sci. Eng.*, 2019, **2019**, 1826148.

48 X. Zhu, B. Liu, H. Hou, Z. Huang, K. M. Zeinu, L. Huang, X. Yuan, D. Guo, J. Hu and J. Yang, Alkaline intercalation of Ti3C2 MXene for simultaneous electrochemical detection of Cd (II), Pb (II), Cu (II) and Hg (II), *Electrochim. Acta*, 2017, **248**, 46–57.

49 W. Wu, M. Jia, Z. Wang, W. Zhang, Q. Zhang, G. Liu, Z. Zhang and P. Li, Simultaneous voltammetric determination of cadmium (II), lead (II), mercury (II), zinc (II), and copper (II) using a glassy carbon electrode modified with magnetite (Fe3O4) nanoparticles and fluorinated multiwalled carbon nanotubes, *Microchim. Acta*, 2019, **186**, 97.

50 F. Wantz, C. E. Banks and R. G. Compton, Edge plane pyrolytic graphite electrodes for stripping voltammetry: a comparison with other carbon based electrodes, *Electroanalysis*, 2005, **17**, 655–661.

51 B. Rezaei, M. Ghiaci and M. E. Sedaghat, A selective modified bentonite–porphyrin carbon paste electrode for determination of Mn (II) by using anodic stripping voltammetry, *Sens. Actuators, B*, 2008, **131**, 439–447.

52 W. Yue, A. Bange, B. L. Riehl, B. D. Riehl, J. M. Johnson, I. Papautsky and W. R. Heineman, Manganese detection with a metal catalyst free carbon nanotube electrode: anodic versus cathodic stripping voltammetry, *Electroanalysis*, 2012, **24**, 1909–1914.